BIOINFORMATICS ORIGINAL PAPER

Vol. 30 no. 12 2014, pages 1747–1754
doi:10.1093/bioinformatics/btu102

Bioimage informatics

Advance Access publication February 18, 2014

# Automated analysis of giant unilamellar vesicles using circular Hough transformation

Eduard Hermann, Stephanie Bleicken, Yamunadevi Subburaj and Ana J. García-Sáez*

Max-Planck Institute for Intelligent Systems, Heisenbergstr. 3, 70569 Stuttgart and Interfaculty Institute for Biochemistry, University of Tübingen, Hoppe-Seyler-Straße 4, 72076 Tübingen, Germany

Associate Editor: Jonathan Wren

## ABSTRACT

**Motivation:** In order to obtain statistically relevant results, the study of membrane effects at the single-vesicle level requires the analysis of several hundreds of giant unilamellar vesicles (GUVs), which becomes a very time-consuming task if carried out manually. Complete and user-friendly software for fast and bias-free automated analysis has not been reported yet.

**Results:** We developed a framework for the automated detection, tracking and analysis of individual GUVs on digital microscopy images. Our tool is suited to quantify protein binding to membranes as well as several aspects of membrane permeabilization on single vesicles. We demonstrate the applicability of the approach by comparing alternative activation methods for Bax, a pore-forming protein involved in mitochondrial permeabilization during apoptosis.

**Availability and Implementation:** The complete software is implemented in MATLAB (The MathWorks, Inc., USA) and available as a standalone as well as the full source code at http://www.ifib.uni-tuebingen.de/research/garcia-saez/guv-software.html.

**Contact:** ana.garcia@uni-tuebingen.de

**Supplementary information:** Supplementary data are available at *Bioinformatics* online.

Received on November 21, 2013; revised on February 3, 2014; accepted on February 11, 2014

## 1 INTRODUCTION

In recent years, giant unilamellar vesicles (GUVs) have become powerful and widely used tools to study membrane processes (Apellaniz *et al.*, 2010a, b; Baumgart *et al.*, 2003; Bleicken *et al.*, 2013a, b; Garcia-Saez *et al.*, 2009; Jalmar *et al.*, 2010; Klose *et al.*, 2010; Leduc *et al.*, 2004; Roux *et al.*, 2010; Schon *et al.*, 2008; Wollert and Hurley, 2010). Among other applications, GUVs are extensively used to investigate the mechanisms of pore-forming molecules (Alam *et al.*, 2012; Apellaniz *et al.*, 2010a; Bleicken *et al.*, 2013a, b; Fuertes *et al.*, 2010; Garcia-Saez *et al.*, 2009; Kawai *et al.*, 2013; Lee *et al.*, 2008; Praper *et al.*, 2011; Schon *et al.*, 2008; Steringer *et al.*, 2012; Tamba *et al.*, 2007; Tamba and Yamazaki, 2005, 2009; Wheaten *et al.*, 2013a, b). In previous work, we developed a GUV-based single-vesicle method for the analysis of membrane permeabilization (Apellaniz *et al.*, 2009). The individual-vesicle integrity, the permeabilization degree, the stability of the permeabilized state, the binding of proteins to the membrane as well as the kinetics of single-vesicle leakage can be successfully addressed with this approach (Apellaniz *et al.*, 2010a; Bleicken *et al.*, 2013a, b; Fuertes *et al.*, 2010; Steringer *et al.*, 2012).

However, to achieve high statistical accuracy, several hundreds of GUVs per experiment need to be considered. The analysis of GUV experiments is mostly carried out on digital microscopy images using basic image processing techniques like measuring mean pixel intensities on defined regions of interest or quantifying certain shape features (Alam *et al.*, 2012; Apellaniz *et al.*, 2009; Bergstrom *et al.*, 2013; Bleicken *et al.*, 2013a, b; Garcia-Saez *et al.*, 2009; Mally *et al.*, 2002; Tamba *et al.*, 2007; van Rooijen *et al.*, 2010). Due to the high amount of vesicles, this method usually turns out to be extremely time consuming and can additionally suffer from subjective bias if carried out manually. The researcher might tend to select GUVs following certain characteristics like size or degree of filling and thus introduce a bias into the sample.

So far, integrated systems for segmenting large populations of lipid vesicles are scarce in publishing research. Zupanc *et al.* (2011) proposed a vesicle segmentation algorithm based on the Markov random field model, which depends on a bright vesicle rim and a generous intensity contrast between the inner and outer region of the vesicle. This is hardly the case in permeabilization studies since a reduced dye concentration and laser power during image acquisition is required to not considerably affect membrane properties.

We propose the Circular Hough Transformation (CHT), a robust technique to find circular patterns in images (Duda and Hart, 1972), for the segmentation of GUVs and demonstrate its efficiency on noisy real experiment images. To our best knowledge, this article presents the first complete and user-friendly framework for the automated detection and analysis of large GUV populations. It is suitable for an entire permeabilization analysis, including kinetics and the size and stability of pores. In addition, radial profiles for each vesicle can be used to acquire quantitative information about protein binding to membranes. The automatization is not only advantageous in terms of time saving, but also guarantees an unbiased statistical analysis to the highest possible extent. The software is therefore powerful not only in detecting circular objects in microscopy images, but also objects which moderately deviate from the circular shape. For the analysis of movies, we implemented a tracking algorithm which allows tracking of single vesicles, making the software applicable to moving GUVs.

To validate the approach and demonstrate the applicability of our program, we investigated the degree of individual vesicle

*To whom correspondence should be addressed.

permeabilization induced by Bax under different activating conditions. Bax is a member of the Bcl-2 family with a major role in the regulation of apoptosis. It induces the permeabilization of the outer mitochondrial membrane (OMM) that releases cytochrome c (cyt c) during apoptosis (Garcia-Saez *et al*., 2010). Despite intense research, the mechanism of Bax-induced OMM permeabilization is under debate. Previous studies showed that the cleaved form of the BH3-only protein Bid activates Bax (Chipuk *et al*., 2006; Kuwana *et al*., 2005; Letai *et al*., 2002; Li *et al*., 1998). Furthermore, Bax activation has been shown to occur in vitro by incubation with detergents, acid pH or high temperature (Antonsson *et al*., 2000; Hsu and Youle, 1997, 1998; Kuwana *et al*., 2002; Suzuki *et al*., 2000). But whether these methods induce comparable Bax activation and pore activity remains unknown. In this article, we compared the effect of these four activating methods on Bax-induced membrane permeabilization at the single-vesicle level. Our results demonstrate that all four methods efficiently activate Bax and yield comparable all-or-none pore activity on cardiolipin-containing GUVs.

## 2 GENERAL FEATURES

### 2.1 Pre-processing

Raw images as acquired under real conditions are usually not optimally suited for segmentation but require some pre-processing. Most GUV images have a poor contrast due to low dye concentration and laser power (as usually desired to avoid artifacts). On the other hand, the GUV-detection algorithm is initialized by the detection of edges, which is best carried out on a high-contrast image. Thus as a crucial step, contrast is increased by linear mapping of a user-defined gray-value interval ($I_{\min}$; $I_{\max}$) to the maximally representable grayscale range. Values below $I_{\min}$ are mapped to 0 and those above $I_{\max}$ to the highest possible gray-value. Additionally, we found that slight smoothing contributes to an increased detection performance. From our experience, convoluting the image with a boxcar filter to smooth out short-scaled noise works best on fluorescent microscopy images.

For high processing speed it is convenient to minimize the file size as much as possible but a limit to this procedure is given by the accuracy of object localization and gray-value determination. On the image, even the smallest GUVs must have a size that is much larger compared to the size of one pixel. In our experience and considering typical GUV sizes, resizing to a resolution of 1.7 pixels/μm seems to be a good choice. The applied resizing mechanism is based on the bicubic interpolation.

### 2.2 Automatic detection of GUVs

The detection algorithm is based on the CHT, a model-based method for the segmentation of circular shapes in images. The CHT mainly consists of a voting process, where every point in the image votes for a point in an accumulation array according to a specific voting scheme. Image points belonging to a circular-shaped object vote for the same point in the accumulation array, leading to local maxima. The detection of circles is then reduced to the task of detecting peaks in the accumulation array (see Supplementary Material for a more detailed description of the CHT).

Parallel to the classical CHT method provided by Matlab, we use a variation of the Adaptive Hough Transform (Illingworth and Kittler, 1987; Peng *et al*., 2007; Zupanc *et al*., 2010). Some GUVs are detected only by one of both methods but based on our experience we could not figure out if one of the methods works generally better on our images than the other. The parallel arrangement of both CHT algorithms maximizes the detection efficiency by providing the set union of the individual results. In case that one GUV is detected by both methods, one of the counts is eliminated; the requirement for such discrimination is that the distance between the center points is less than the sum of the radii of both GUVs.

Figure 1B and C show the final accumulation array for a typical GUV image (Fig. 1A) in 2D and 3D, respectively. The peaks clearly indicate the positions of the GUVs. The tool is not only restricted to detect perfectly spherical vesicles but can also deal with objects which slightly deviate from the circular shape, for instance ellipses. In Figure 1D we used one of the images obtained from the same experiment as Figure 1A and stretched it by a factor of 1.5 in horizontal direction. As a result, the GUVs appear as ellipses instead of circles. Our tool detected 22 objects from which two were false detections and two objects were missing.

The circle detection is the key process and the raw output, consisting of center points and radii, can be used for several kinds of pixel-based analysis. Our program is specialized to determine mean intensities within circles as well as radial intensity profiles, but the implementation of other analysis schemes is straightforward.

### 2.3 GUV tracking in image sequences

When dynamic processes are of interest, time series can be recorded resulting in stack files with several frames, usually >100. Normally, the vesicles change their position from frame to frame due to Brownian diffusion. Moreover, GUVs can diffuse into or out of the observed sample region, leading to a changing number of detections among the frames. Particle tracking plays an important role in biosciences when time-lapse experiments are performed on moving particles (Sbalzarini and Koumoutsakos, 2005). We implemented a tracking algorithm to follow the movement of single vesicles through the image sequence. The GUV-detection algorithm is applied to each frame and yields a set of $T$ (total number of frames in the image sequence) matrices $C^t$ with rows $\left[x_p, y_p\right]_{p=1}^{N_t}$, where $N_t$ is the total number of detected GUVs in frame $t$ and $(x_p, y_p)$ are the coordinates of the center point of one GUV. The tracking tool identifies detection points corresponding to the same GUV in subsequent frames.

Let $\Im$ represent the set of detection points $p_i\,(i = 1, ..., N_t)$ in frame $t$ and $R$ a user-defined integer parameter specifying how many future frames are to be considered. For all sets $\aleph_r, r = 1, ..., R,$ of detection points $q_j$, where $j = 1, ..., N_{t+r}$ in frame $t+r$, an association matrix $G_r^t$ is defined as $G_r^t(i,j) = 1$ if $p_i$ in frame $t$ and $q_j$ in frame $t+r$ are produced by the same vesicle and $G_r^t(i,j) = 0$ otherwise. Every row and every column of $G_r^t$ can contain maximally one entry of value 1, all others are 0. The detection points $p_i$ and $q_j$ are associated to the same GUV if the distance between their center points is smaller than for any other possible association and is at the same time below a user-defined threshold.

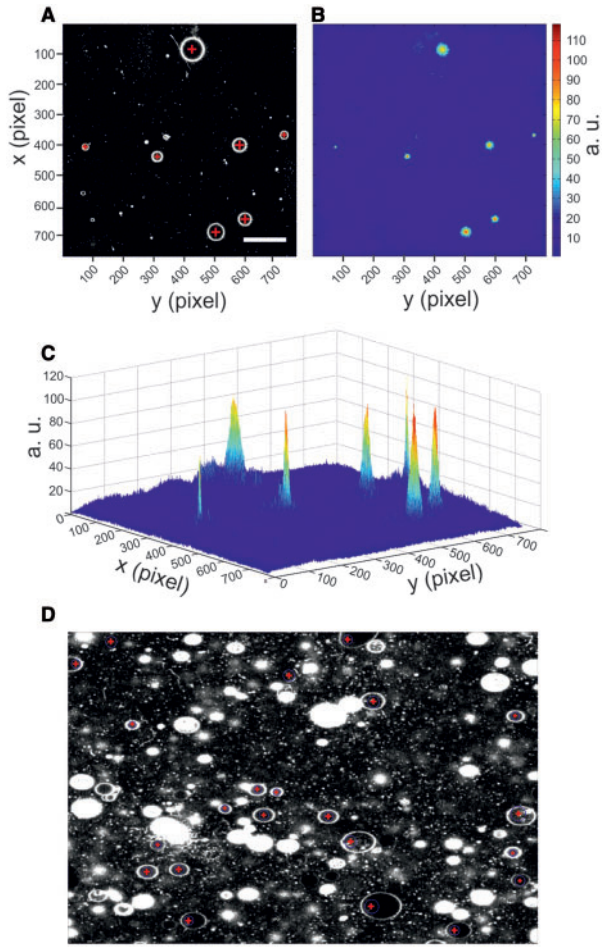


**Fig. 1.** CHT is used to find GUVs on confocal microscopy images. (A) GUVs are detected automatically by applying the CHT. Each vesicle detected is marked with a red cross. Scale bar: 100 µm. Signal-to-noise ratio: 25:1. The GUVs were prepared by electroformation (Angelova and Dimitrov, 1986) and were composed of PC/CL (4:1) with <0.05% DiO used as lipid marker. All images are single confocal images. The extension of the focal volume in $z$-direction is 2 µm. (B and C). In the detection process, the accumulation array (matrix) has the same size as the original image and contains real numbers which are initially all set to 0. The voting process of the CHT leads to a pattern where maxima correspond to the center positions of the GUVs. Detecting GUVs is reduced to the task of finding maxima in the accumulation array. (D) The program is also suitable to detect objects which are not perfectly round. By stretching one of the images from the same experiment by a factor of 1.5 in horizontal direction, the vesicles appear as ellipses. The automatic detection yields a total amount of 22 identified objects in the shown image, from which two were false detections, while two objects remained undetected. The bright spots are MLVs containing lipids in their interior. Ideally, only true GUVs contribute to the permeabilization result, while MLVs are excluded from the analysis by thresholding the inner pixel intensity of the vesicles in the membrane channel

If for one $r>1$ we have $G_r^t(i,j)=1$ but $G_{r'}^t(i,j)=0$ for all $r'=1,\ldots,r-1$, it means that a GUV was successfully detected in frame $t$ and frame $t+r$, but not in the intermediate frames. Nevertheless we assume that the GUV is also present in the intermediate frames but is missing in the result due to limited detection efficiency. In this case, the missing detection points are automatically added to the intermediate frames. The center point $\vec{x}_{r+t'}$ of a missing vesicle in frame $t+r'$ is set to $\vec{x}_{t+r'}=\vec{x}_t+\frac{r'}{r}\left(\vec{x}_{t+r}-\vec{x}_t\right)$ and the radius $R_{t+r'}$ to $R_{t+r'}=[(r-r')R_t+r'R_{t+r}]/r$. Accordingly, we set $G_{r'}^t(i,j)=1$ for all $r'=1,\ldots,r-1$.

Let $t$ and $t'$ be frames, $t'>t$. Then the one-elements of the matrix product $B_{tt'}=\prod_{i=t}^{t'}G_1^i$ connect the detection points between the two frames. $B_{tt'}(i,j)=1$ means that the $i$-th detection in frame $t$ and the $j$-th detection in frame $t'$ are produced by the same GUV.

## 2.4 Automated pixel-based analysis

Usually, when imaging GUVs, more than one fluorophore is used and thus the image file consists of stacks containing several channels. In order to perform unbiased GUV detection, one channel should contain the fluorescence signal of the vesicle membrane and the detection step is performed only in this channel. Once the center points and radii are obtained, they can in principle be used for any kind of further pixel-based analysis on the additional channels of the stack file. For the permeabilization analysis, the percentage of GUV filling is given by

$$P=100\times\frac{F^{\text{in}}-F_0}{F^{\text{out}}-F_0} \tag{1}$$

where $F^{\text{in}}$ and $F^{\text{out}}$ are the average fluorescence intensities inside and outside a GUV, and $F_0$ is the initial fluorescence signal inside the GUV or noise offset. Along this article, we will usually refer to $F^{\text{out}}$ as background and to $F_0$ as offset.

The background as well as the offset is determined separately for each channel and frame to preserve intensity variations across the image. For the automated determination of the background intensity, the algorithm first smoothes the image with a boxcar filter of 1/50 of the original image size. The most frequent gray-value in the smoothed image is reported as background intensity. The offset is estimated by collecting pixel intensities within non-permeabilized GUVs, as they provide regions where no free dye but only noise contributes to the local fluorescence intensity. To keep GUV pixels separate from background and considering typical GUV diameters, we smooth with a smaller boxcar filter, having 1/90 of the original image size. The average over the 1000 darkest pixels is reported as offset.

Unlike the detection which is performed on one specified channel, the analysis of percentage of GUV filling according to Equation (1) is carried out on all channels. This allows for performing a variety of analysis, like total permeabilization, permeabilization kinetics or estimation of pore stability and size (Apellaniz *et al.*, 2011; Bleicken *et al.*, 2013 a, b; Steringer *et al.*, 2012). For example, the histogram of permeabilization degrees of a GUV population provides insight into the mechanism of pore formation, while the permeabilization kinetics can be used to estimate the total permeabilized area per GUV.

Figure 2 shows some example measurements that can be analyzed with the presented program. Time-lapse image sequences allow the observation of the GUV-filling process with time and can be used to characterize the permeabilization kinetics (Fig. 2A). The ability to read out intensities at the same position in different channels can be mostly used for studying the stability

of the permeabilized state and estimating the pore size, as explained in Figure 2B. Moreover, the program analyzes the radial profile of each vesicle, which provides mean pixel values along a circle perimeter as a function of the radius. This function is suitable to quantify protein binding to GUV membranes. If the protein of interest, fluorescently labeled, binds to the membrane, a peak of fluorescence intensity appears on the GUV boundary (Fig. 2C).

The algorithm automatically discriminates multi-lamellar vesicles (MLV) since they are not of interest for permeabilization measurements. Due to their multiple-labeled lipid bilayers, they are characterized by high inner-pixel intensity in the membrane channel and are excluded from the analysis by simple thresholding.

### 2.5 Manual control of the automated analysis

The program presented here includes several options to control manually the quality of the analysis. These options are accessible via the graphical user interface we provide (Supplementary Figure S1) and are explained in detail in the user manual which we provide together with the software. False detections can be removed fast and easily by clicking on them and pressing the Remove button. On the other hand, the user can manually add undetected GUVs by dragging a mask over the region of interest and defining this region as a new GUV. Background and offset intensities can be modified by hand at any time during the analysis. Even when the data are already analyzed, a change in background or offset prompts the program to recalculate the data. Additionally, the user can collectively scale the radius of the GUVs by a factor of his choice. This is especially useful if small vesicles with diameters <20 pixels dominate the image. Then, the size of the region of interest for measuring the inner pixel intensity has to be chosen generously smaller than the GUV itself to ensure that no background is included in the region of interest. A rescaling of the radii by a value between 0.4 and 0.8 is highly recommended in this case.

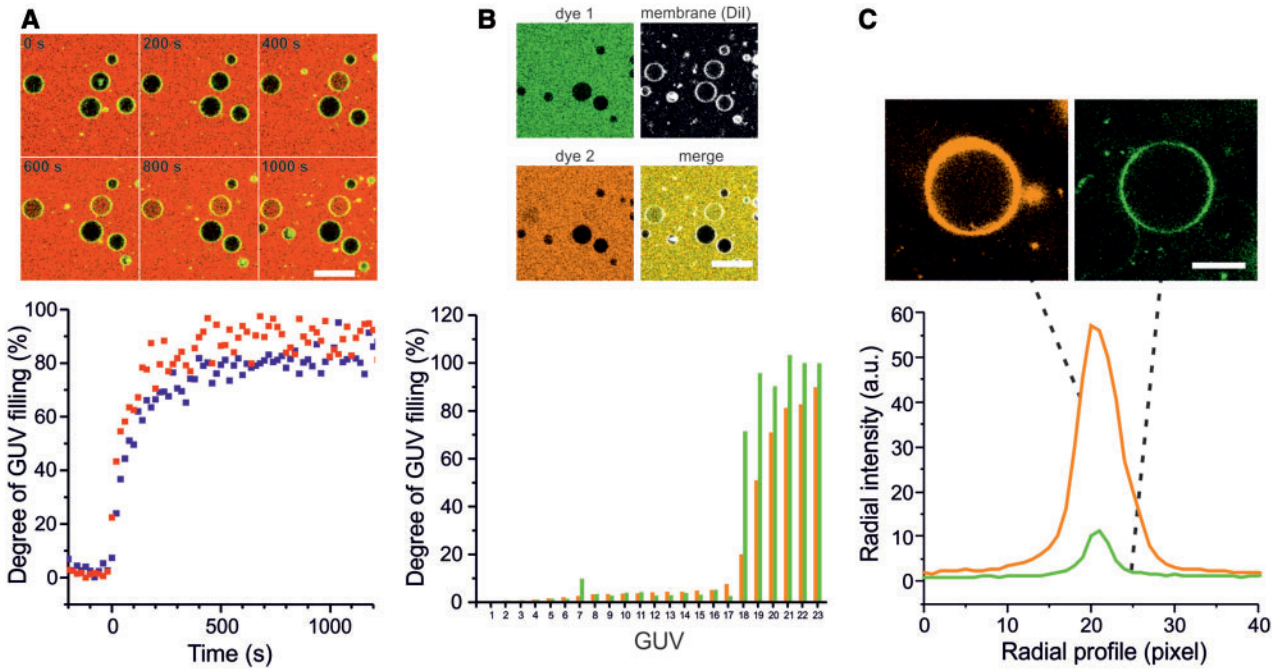


**Fig. 2.** The automated GUV analysis tool is suited to analyze image sequences (movies) and multichannel images. In all cases, the detection of the GUVs is performed on a user-selected channel. Generally, the membrane channel should be used for an unbiased detection. The mean pixel intensity is read out on the obtained regions of interest (interior of vesicles) in all channels and frames. (A) Taking an image sequence during an experiment of GUV permeabilization allows the observation of the filling kinetics. Here, two independent GUVs (red and blue) were observed every 20 s for 1000 s. Scale bar: 30 µm. (B) The multichannel analysis can be used to characterize the pore size and pore stability. For pore size, two free dyes with different molecular sizes are added simultaneously and the degrees of filling for both dyes are compared. Cyt c (12 kDa) can be used as dye 1 and APC (105 kDa) as dye 2, for instance (Bleicken *et al.*, 2013b). For pore stability, different free dyes with similar chemical properties are added at different times during incubation. A stable pore remains open once it is formed and allows the internalization of all dyes. To demonstrate the principle of the multichannel analysis, we used here Alexa488 (dye 1) and Alexa633 (dye 2), which have the same size and were added at different time points, and analyzed 23 GUVs composed of PC/CL (4:1) with <0.05% DiO. The fact that the permeability of the individual vesicles is essentially the same for both dyes indicates that the pores are stable. If this were an experiment to test pore size, the conclusion would be that the pores are large enough to allow the entry of both dyes. To make a statistically significant conclusion, independent repetitions and a large number of vesicles (>100 per repetition) are needed. Scale bar: 30 µm. (C) Radial profiles are created for all GUVs in a user-defined channel. The pixel intensity averaged over a circle perimeter (*y*-axis) is recorded as a function of the circle radius (*x*-axis), starting at the GUV center point and reaching up to the doubled GUV radius. The radial profiles of a bright and a dark GUV are shown as examples. Both vesicles have a radius of 20 pixels and the zero-position was set to the vesicle center. This method can be used, for instance, to quantify protein binding to the membrane. Here, the radial intensity originates from DiO in the vesicle membrane. Scale bar: 10 µm

## 3 METHOD VALIDATION

### 3.1 Finding an optimal set of parameters

We first tested the performance of our tool for different parameter sets on a training image from the same experiment as used for the evaluation in Figure 3. Therefore we compared the efficiency of the automatic GUV detection, namely the number of correctly detected GUVs and the number of false detections (detections which do not correspond to GUVs). For the permeabilization study, only undistorted GUVs are desired to contribute to the result, since they are well-defined structures. No MLVs should be included.

Table 1 shows the effect of the user-defined parameters, namely the contrast adjustment and the radius range, on the detection result. A high contrast is favorable for a good detection rate but exorbitant contrast enhancement would saturate a large number of pixel values and reduce the detection performance. In our experiments, we labeled the vesicle membrane with 0.05% DiO and adjusted the laser power so that the GUVs can still be seen on the microscope (30–200 μW). Under these conditions, we found best if pixel values ranging from 0 to 30 (with 255 being the highest pixel value) are mapped to the full representable range of pixel intensity.

For the radius range, a default of 10–50 pixels is predefined in the GUI and works best for GUVs prepared following the proposed protocol (Angelova and Dimitrov, 1986) and an image resolution of 2.4 pixels/μm. In general, the minimum radius should not be set below 10 pixels since it is not possible to measure the fluorescence intensity within smaller GUVs with sufficient accuracy. On the other hand, choosing a maximum radius >50 pixels is only recommended in the absence of small GUVs. Otherwise, the CHT tends to misinterpret accumulations of small vesicles as one huge GUV, if those accumulations have a roughly circular shape. However, we did not observe this effect using the default radius range.

MLVs are excluded from the analysis by a user-defined threshold for the intensity of the vesicle interior in the membrane channel. To determine the most appropriate threshold value, we measured typical MLV intensities using the manual tools provided in the GUI and arrived at a best value of 7 (total range is 0–255). Additionally, the user has the possibility to scale down the size of all masks where the pixel intensity within the GUVs is read out. We encourage the user to test for different scaling factors prior to saving the analysis result. Proper scaling will ensure that no background pixels contribute to the result. For the training image, a scale factor of 0.45 was the best choice. Assuming a homogenous dye distribution within the GUVs, an underestimation of the scaling factor has no effect on the permeabilization histogram. On the other hand, an overestimation will shift the histogram towards high permeabilization values since background pixels are included in the masks.

Even when the best parameter set is found, some GUVs may still remain undetected, which is mainly due to the following reasons.

- Brightness: one particular GUV may contain less dye on its membrane than the majority of the vesicles in the image. As a result, it shows less fluorescent intensity and will probably not be matched by the Hough Transformation. To avoid this, the experimentalist should mix well the lipid

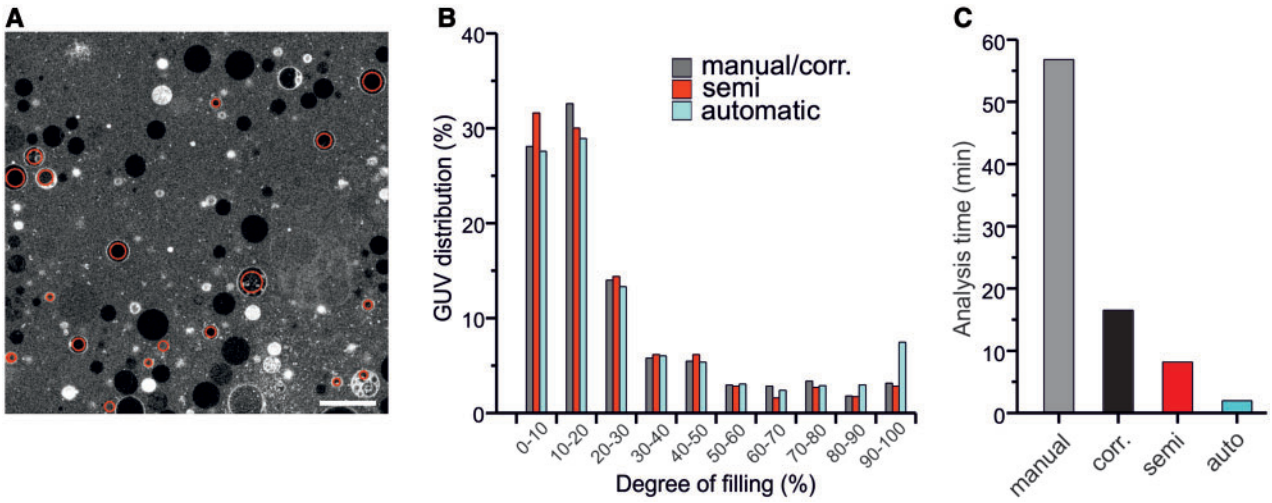


**Fig. 3.** Comparison of automated and manual GUV analysis. Five images like (A) with a total amount of 200 GUVs were used to compare the automatic with the manual analysis. The internalization of free dye into the lumen of the individual vesicles indicates membrane permeabilization. In all cases, the degree of GUV filling was determined based on the ratio of averaged inner and outer pixel intensity. The GUV images were generated after 90 min of incubation with Bax. Scale bar: 100 μm. Signal-to-noise ratio: 8:1. (B) Distribution of the degree of filling of the GUVs analyzed with three different methods: (i) automatic: the parameters were optimized for best detection efficiency and the result was not corrected for false detections or missing GUVs; (ii) semi-automatic: false positives were removed from the result of the automatic analysis; (iii) manual/corr.: undetected GUVs were added to the result of the semi-automatic analysis. This corresponds to a complete manual analysis as it has been commonly used in GUV experiments up to now. The automatic method provided 167 detections. Forty-seven detections were false positives and 80 GUVs remained undetected. (C) Comparison of the analysis time: the automatic analysis is 20 times faster than the manual analysis. Corr. means the automatic analysis with subsequent removal of false positives and adding of undetected GUVs. This method provides the same result as the manual analysis but is still around three times faster

**Table 1.** GUV detection performance for different parameter sets

| Parameters | | Results | |
|---|---|---|---|
| Contrast range (intensity values) | Radius range (pixel units) | Detected GUVs | False detections |
| 0–30 | 10–50 | 120 | 15 |
| 0–20 | 10–50 | 111 | 15 |
| 0–40 | 10–50 | 110 | 15 |
| 0–30 | 15–50 | 90 | 13 |
| 0–30 | 10–60 | 112 | 18 |

A training image containing 133 GUVs from the same experiment as in Figure 3 was used to compare the detection performance for different parameter sets. For contrast, the indicated range of intensity values is linearly mapped to the full range of 0–255. Radius range is given in pixel units (image resolution is 2.4 pixels/μm). The first line shows the optimal parameter set, giving the best balance between high number of detected GUVs and low number of false detections. Since it is easier to manually remove a false detection than to add a missing GUV, we assign more weight to the number of detected GUVs

composition with the lipophilic dye to achieve a homogeneous dye distribution. As the dye concentration is generally low (<0.05% DiO, for instance), small differences in the concrete amount of dye on the membrane is not supposed to affect the permeabilization behavior of the GUVs. Thus, no bias is expected when those vesicles remain undetected.

- Size: the CHT requires a user-defined radius range for the search of circular objects. We recommend a range of 10 to 50 pixels for image resolutions of ~2.4 pixels/μm and using the electroformation protocol suggested in this manuscript (Angelova and Dimitrov, 1986). Some large GUVs are beyond this range and remain undetected, but can be easily added manually. Anyway, they are not expected to have a different permeabilization behavior compared to the rest of the GUVs. However, in cases where proteins influence the size of the GUVs, the software could add bias by preferably analyzing a certain size range. This needs to be considered by the researcher.
- Distorted shape: if carried out carefully, the electroformation produces circular GUVs. Otherwise, some vesicles deviate from the circular shape. As demonstrated in Figure 1D, our tool also detects distorted shapes like ellipses, but with lower efficiency compared to circles. A slight deviation from the circular shape should in principle not affect the ability of vesicles to permeabilize. In some cases it is even advantageous to exclude distorted GUVs from the analysis (for example for the estimation of vesicle radii).

### 3.2 Comparison of manual and automatic analysis

The quality of the automated GUV detection and analysis was evaluated using a set of images from real experiments. The degree of membrane permeabilization was directly determined by monitoring the entry of a dye into the lumen of the GUVs initially devoid of dye (Fig. 4A). The extent of permeabilization can be quantified for individual vesicles on the sample. This allows the identification of subpopulation effects, which is not possible in traditional bulk experiments. To analyze the goodness of our automated GUV analysis, we compared the extent GUV permeabilization obtained in the experiments with three different analysis methods: (i) automatic analysis without any manual interaction except for eventual background/offset correction or radius rescaling, (ii) a semi-automatic analysis which consists of the first method followed by manual removal of false positives and (iii) the second method followed by manual adding of missing GUVs. Note that the third analysis mode provides the same result as a completely manual analysis since it includes all possible manual corrections. Figure 3 shows the direct comparison of all three methods in terms of population analysis of the degree of single GUV permeabilization, as well as the required analysis time for a set of images containing GUVs after incubation with inactive Bax. Totally, our test images contained 200 GUVs. The permeabilization distribution differs only slightly among the methods and in all cases leads to the same conclusions for the experiment (Fig. 3B). In this comparison, the automatic method provides a higher fraction of highly permeabilized GUVs (with >90% filling degree) than the manual and the semi-automatic methods. This is mainly due to false detections, which do not correspond to vesicles but to background, thus yielding a higher fraction of reputedly fully permeabilized GUVs.

Comparing the analysis time, we find important differences between the pure manual analysis and the three methods making use of our tool (Fig. 3C). Without any manual corrections, one can save ~95% of analysis time compared to the manual analysis, while achieving a very similar result. Even for full corrections, which provide the same result as the manual analysis, one still saves ~70% of analysis time. From our results, we estimate an averaged analysis speed for one image of around 80 GUVs per minute on a common desktop computer with 3.40 GHz and 16 GB RAM, compared to ~6 GUVs per minute for manual analysis.

It is notable that this high level of accuracy is achieved by detecting only 60% of available GUVs compared to the manual analysis. In our evaluation experiment, the pure automatic detection provided 167 GUVs; 47 of them were false positives and 80 GUVs could not be detected automatically. This robustness of the method is due to the fact that the number of GUVs belonging to a certain class (e.g. bin of 10% of degree of filling as in our analysis) follows a Poisson distribution and, as a result, the error of the measurement depends on the square root of the number of GUVs. For this reason, in order to obtain high statistical accuracy, not the fraction of detected GUVs is of importance, but the absolute number of data points. From our experience, analyzing ~100 GUVs per experiment is already sufficient for a representative result. Adding more GUVs to the analysis will cause only a slight increase in statistical accuracy, which is in most cases irrelevant compared to the systematic error of the individual experiment. In most applications, the semiautomatic analysis is a good balance between fast processing and accurate results.

### 3.3 Different methods of Bax activation yield similar permeabilization of GUVs

We validated and demonstrated the applicability of the automated GUV analysis tool by testing the permeabilization of

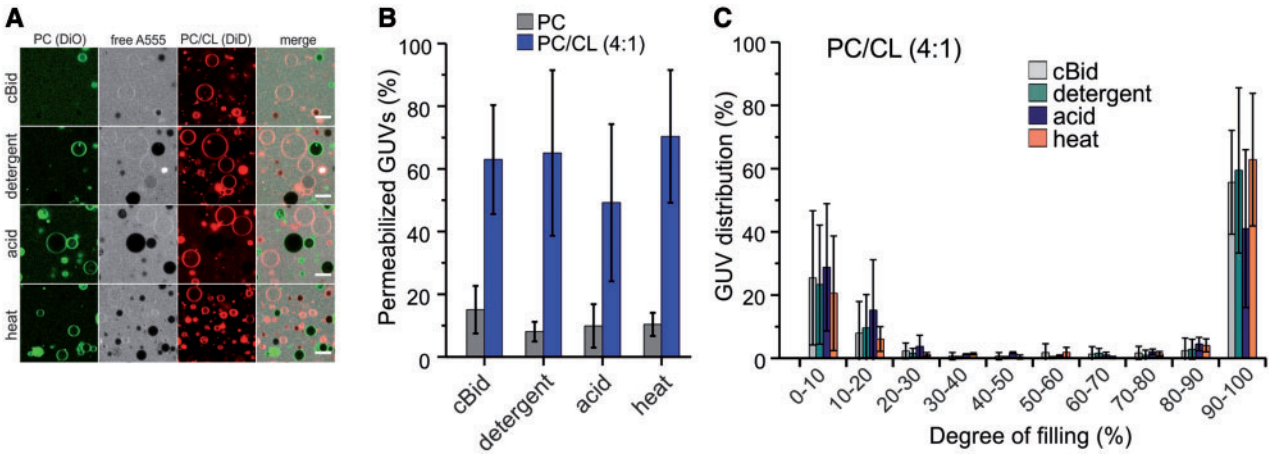


**Fig. 4.** Incubation with cBid, detergent, acidic pH or at 42°C induce comparable activation of Bax and GUV permeabilization. (A) The internalization of Alexa555 into the lumen of the individual vesicles indicates membrane permeabilization. Green GUVs are composed of PC, and red GUVs are made of PC/CL (4:1). Images were taken 90 min after mixing the components (30 min for the heating experiment). Scale bar: 30 μm. (B) Fraction of permeabilized GUVs (with a degree of filling >50%). (C) Distribution of filling degrees of GUVs after 90 min of incubation (30 min for the heat experiment). GUVs were composed of PC/CL (4:1). Each experiment was repeated three times and in each of three repetitions, a minimum of 100 GUVs were analyzed. Error bars correspond to the standard deviation. Bin size is 10%

GUVs induced by Bax using different methods of activation. GUVs composed of pure PC or PC/CL (4:1) were visualized using lipophilic dyes of different colors (DiO, green and DiD, red), mixed in a buffer-containing free Alexa555 and Bax at 20 nM, and incubated under four different conditions (Fig. 4A): (i) in the presence of cBid, (ii) in the presence of detergent, (iii) at pH 5.5 and (iv) at $T = 42°C$ (experiments (i), (ii) and (iii) were performed at room temperature). The experimental details are described in the Supplementary Material.

By mixing GUVs of different lipid compositions, preferences for certain membrane types can be directly assessed in a situation closer to the coexistence of membranes in a cell. For all conditions, we observed permeabilization of vesicles containing CL, but not with pure PC, illustrating the effect of the mitochondrial lipid CL on the membrane activity of Bax (Fig. 4B and C). It is notable that with all activation protocols, similar all-or-none permeabilization was observed. Comparable results were obtained when CL was substituted by PG (data not shown), indicating that rather than a specific CL effect, negatively charged lipids are necessary and enough for Bax pore activity. Supplementary Figure S3 shows the corresponding control experiments.

Our results suggest that all four methods of Bax activation promote a similar mechanism of pore formation. This all-or-none mechanism is likely associated with a cooperative transition from a closed to an open state.

## 4 CONCLUSIONS

In this article, we presented a computationally efficient and robust method for the detection and analysis of GUVs based on the CHT. The algorithm is not intrinsically limited to GUVs. In principle, giant vesicles produced from the plasma membrane of cells or any other circular objects can be detected according to the applicability of the CHT. Even distorted circular objects can be segmented and analyzed with our tool. It can be used for quantitative studies of vesicle size, membrane permeabilization and protein binding on a single-vesicle level. Also time-lapse analysis can be performed even if the vesicles move during the measurement time. We showed that the automated-GUV-analysis platform is of high accuracy on noisy real microscopy images taken usually at low laser power and low dye concentration. The results obtained from the analysis of experiments of GUV permeabilization using our application were comparable to the results obtained in a time consuming manual analysis. Even if the automatic analysis was complemented by manual corrections to match all available GUVs, the time saving is still ~70% compared to a complete by-hand analysis. The reduced analysis time is of special importance in a single vesicle approach since a high number of GUVs is needed for statistical accuracy.

To validate the application in a real situation, we used it to study GUV permeabilization induced by Bax activated by cBid, detergent, acid or heat. Histograms of permeabilization values of a GUV ensemble are characteristic for the molecular mechanism forming the basis of membrane permeabilization. We observed that all four methods yield all-or-none permeabilization of CL-containing membranes, indicating that regardless the method of activation, the mechanism of pore formation by Bax is maintained.

## ACKNOWLEDGEMENTS

We thank J. Unsay for useful discussions and C. Stegmüller for technical support.

*Funding*: Max Planck Society; German Cancer Research Center; German Ministry for Education and Research (BMBF, grant N.0312040).

*Conflict of Interest*: none declared.

## REFERENCES


Alam,J.M. *et al.* (2012) The single-giant unilamellar vesicle method reveals lysenin-induced pore formation in lipid membranes containing sphingomyelin. *Biochemistry*, **51**, 5160–5172.

Angelova,M.I. and Dimitri,D.S. (1986) Liposome electroformation. *Faraday Disc. Chem. Soc.*, **81**, 303–311.

Antonsson,B. *et al.* (2000) Bax oligomerization is required for channel-forming activity in liposomes and to trigger cytochrome c release from mitochondria. *Biochem. J.*, **345**, 271–278.

Apellaniz,B. *et al.* (2010a) All-or-none versus graded single-vesicle analysis reveals lipid composition effects on membrane permeabilization. *Biophys. J.*, **99**, 3619–3628.

Apellaniz,B. *et al.* (2010b) Confocal microscopy of giant vesicles supports the absence of HIV-1 neutralizing 2F5 antibody reactivity to plasma membrane phospholipids. *Febs Lett.*, **584**, 1591–1596.

Apellaniz,B. *et al.* (2011) Destabilization exerted by peptides derived from the membrane-proximal external region of HIV-1 gp41 in lipid vesicles supporting fluid phase coexistence. *Biochimica Et Biophysica Acta-Biomembranes*, **1808**, 1797–1805.

Apellaniz,B. *et al.* (2009) Distinct mechanisms of lipid bilayer perturbation induced by peptides derived from the membrane-proximal external region of HIV-1 gp41. *Biochemistry*, **48**, 5320–5331.

Baumgart,T. *et al.* (2003) Imaging coexisting fluid domains in biomembrane models coupling curvature and line tension. *Nature*, **425**, 821–824.

Bergstrom,C.L. *et al.* (2013) Cytochrome c causes pore formation in cardiolipin-containing membranes. *Proc. Natl Acad. Sci. USA*, **110**, 6269–6274.

Bleicken,S. *et al.* (2013a) Mechanistic Differences in the Membrane Activity of Bax and Bcl-xL Correlate with Their Opposing Roles in Apoptosis. *Biophys. J.*, **104**, 421–431.

Bleicken,S. *et al.* (2013b) Proapoptotic Bax and Bak proteins form stable protein-permeable pores of tunable size. *J. Biol. Chem.*, **288**, 33241–33252.

Chipuk,J.E. *et al.* (2006) Mitochondrial outer membrane permeabilization during apoptosis: the innocent bystander scenario. *Cell Death Differ.*, **13**, 1396–1402.

Duda,R.O. and Hart,P.E. (1972) Use of the Hough transformation to detect lines and curves in pictures. *Commun. ACM*, **15**, 5.

Fuertes,G. *et al.* (2010) Pores formed by bax alpha 5 relax to a smaller size and keep at equilibrium. *Biophys. J.*, **99**, 2917–2925.

Garcia-Saez,A.J. *et al.* (2009) Membrane promotes tBID interaction with BCL(XL). *Nat. Struct. Mol. Biol.*, **16**, 1178–1185.

Garcia-Saez,A.J. *et al.* (2010) Permeabilization of the outer mitochondrial membrane by Bcl-2 proteins. *Adv. Exp. Med. Biol.*, **677**, 91–105.

Hsu,Y.T. and Youle,R.J. (1998) Bax in murine thymus is a soluble monomeric protein that displays differential detergent-induced conformations. *J. Biol. Chem.*, **273**, 10777–10783.

Hsu,Y.T. and Youle,R.J. (1997) Nonionic detergents induce dimerization among members of the Bcl-2 family. *J. Biol. Chem.*, **272**, 13829–13834.

Illingworth,J. and Kittler,J. (1987) The adaptive hough transform. *IEEE Trans. Pattern. Anal. Mach. Intell.*, **9**, 690–698.

Jalmar,O. *et al.* (2010) Giant unilamellar vesicles (GUVs) as a new tool for analysis of caspase-8/Bid-FL complex binding to cardiolipin and its functional activity. *Cell Death Disease*, **1**, e103.

Kawai,C. *et al.* (2013) Effects of transmembrane potential and pH gradient on the cytochrome c-promoted fusion of mitochondrial mimetic membranes. *J. Bioenerg. Biomembr.*, **45**, 421–430.

Klose,C. *et al.* (2010) Yeast Lipids Can Phase-separate into Micrometer-scale Membrane Domains. *J. Biol. Chem.*, **285**, 30224–30232.

Kuwana,T. *et al.* (2005) BH3 domains of BH3-only proteins differentially regulate Bax-mediated mitochondrial membrane permeabilization both directly and indirectly. *Mol. Cell*, **17**, 525–535.

Kuwana,T. *et al.* (2002) Bid, Bax, and lipids cooperate to form supramolecular openings in the outer mitochondrial membrane. *Cell*, **111**, 331–342.

Leduc,C. *et al.* (2004) Cooperative extraction of membrane nanotubes by molecular motors. *Proc. Natl Acad. Sci. USA*, **101**, 17096–17101.

Lee,M.T. *et al.* (2008) Mechanism and kinetics of pore formation in membranes by water-soluble amphipathic peptides. *Proc. Natl Acad. Sci. USA*, **105**, 5087–5092.

Letai,A. *et al.* (2002) Distinct BH3 domains either sensitize or activate mitochondrial apoptosis, serving as prototype cancer therapeutics. *Cancer Cell*, **2**, 183–192.

Li,H. *et al.* (1998) Cleavage of BID by caspase 8 mediates the mitochondrial damage in the Fas pathway of apoptosis. *Cell*, **94**, 491–501.

Mally,M. *et al.* (2002) Mechanisms of equinatoxin II-induced transport through the membrane of a giant phospholipid vesicle. *Biophys. J.*, **83**, 944–953.

Peng,T. *et al.* (2007) Algorithms for on-line monitoring of micro spheres in an optical tweezers-based assembly cell. *J. Comput. Inform. Sci. Engineer.*, **7**, 9.

Praper,T. *et al.* (2011) Perforin activity at membranes leads to invaginations and vesicle formation. *Proc. Natl Acad. Sci. USA*, **108**, 21016–21021.

Roux,A. *et al.* (2010) Membrane curvature controls dynamin polymerization. *Proc. Natl Acad. Sci. USA*, **107**, 4141–4146.

Sbalzarini,I.F. and Koumoutsakos,P. (2005) Feature point tracking and trajectory analysis for video imaging in cell biology. *J. Struct. Biol.*, **151**, 182–195.

Schon,P. *et al.* (2008) Equinatoxin II permeabilizing activity depends on the presence of sphingomyelin and lipid phase coexistence. *Biophys. J.*, **95**, 691–698.

Steringer,J.P. *et al.* (2012) Phosphatidylinositol 4,5-Bisphosphate (PI(4,5)P2)-dependent Oligomerization of Fibroblast Growth Factor 2 (FGF2) Triggers the Formation of a Lipidic Membrane Pore Implicated in Unconventional Secretion. *J. Biol. Chem.*, **287**, 27659–27669.

Suzuki,M. *et al.* (2000) Structure of Bax: coregulation of dimer formation and intracellular localization. *Cell*, **103**, 645–654.

Tamba,Y. and Yamazaki,M. (2009) Magainin 2-induced pore formation in the lipid membranes depends on its concentration in the membrane interface. *J. Phys. Chem. B*, **113**, 4846–4852.

Tamba,Y. and Yamazaki,M. (2005) Single giant unilamellar vesicle method reveals effect of antimicrobial peptide magainin 2 on membrane permeability. *Biochemistry*, **44**, 15823–15833.

Tamba,Y. *et al.* (2007) Single GUV method reveals interaction of tea catechin (-)-epigallocatechin gallate with lipid membranes. *Biophys. J.*, **92**, 3178–3194.

van Rooijen,B.D. *et al.* (2010) Membrane permeabilization by oligomeric alpha-Synuclein: in search of the mechanism. *PLoS One*, **5**, e14292.

Wheaten,S.A. *et al.* (2013a) Statistical analysis of peptide-induced graded and all-or-none fluxes in giant vesicles. *Biophys. J.*, **105**, 432–443.

Wheaten,S.A. *et al.* (2013b) Translocation of cationic amphipathic peptides across the membranes of pure phospholipid giant vesicles. *J. Am. Chem. Soc.*, **135**, 16517–16525.

Wollert,T. and Hurley,J.H. (2010) Molecular mechanism of multivesicular body biogenesis by ESCRT complexes. *Nature*, **464**, 864–869.

Zupanc,J. *et al.* (2010) A new approach to analyse effects of nanoparticles on lipid vesicles. *Int. J. Biomed. Nanosci. Nanotechnol.*, **1**, 34–51.

Zupanc,J. *et al.* (2011) Markov random field model for segmenting large populations of lipid vesicles from micrographs. *J. Liposome Res.*, **21**, 315–323.